Accepted Manuscript

In situ structural evolution of arc-deposited Cr-based coatings

A.M. Neves, V. Severo, L. Cvrček, T. Polcar, C. Louro, A. Cavaleiro

PII: S0257-8972(08)00501-X
DOI: doi: 10.1016/j.surfcoat.2008.06.102
Reference: SCT 14396

To appear in: *Surface & Coatings Technology*

Please cite this article as: A.M. Neves, V. Severo, L. Cvrček, T. Polcar, C. Louro, A. Cavaleiro, *In situ* structural evolution of arc-deposited Cr-based coatings, *Surface & Coatings Technology* (2008), doi: 10.1016/j.surfcoat.2008.06.102

This is a PDF file of an unedited manuscript that has been accepted for publication. As a service to our customers we are providing this early version of the manuscript. The manuscript will undergo copyediting, typesetting, and review of the resulting proof before it is published in its final form. Please note that during the production process errors may be discovered which could affect the content, and all legal disclaimers that apply to the journal pertain.

ACCEPTED MANUSCRIPT

IN SITU STRUCTURAL EVOLUTION OF ARC-DEPOSITED Cr-BASED COATINGS

A.M. Neves[a], V. Severo[a], L. Cvrček[b], T. Polcar[c], C. Louro[a] and A. Cavaleiro[a,*]

a) ICEMS, Mechanical Engineering Department, University of Coimbra, 3030-788 Coimbra, Portugal
b) HVM Plasma Ltd., Na Hutmance 2, 158 00 Prague 5, Czech Republic
c) Department of Control Engineering, Faculty of Electrical Engineering, Czech Technical University in Prague, Technická 2, Prague 6, Czech Republic

*corresponding author: albano.cavaleiro@dem.uc.pt

Abstract

Cr-based coatings were prepared by cathode arc evaporation technology using N_2 and C_2H_2 as reactive gases. Three compositions were investigated, $Cr_{60}N_{40}$, $Cr_{41}N_{27}C_{32}$ and $Cr_{67}C_{33}$.

The present investigation is centred on the structural stability via coatings tempering up to 1000ºC, by *in situ* X-ray diffraction in inert atmosphere. As-deposited coatings present low order structure with a medium feature size less then 10 nm. The hexagonal β-Cr_2N phase, characteristic of binary $Cr_{60}N_{40}$ coating, was stable up to 900ºC, before recrystallization and grain growth takes place. For $Cr_{41}N_{27}C_{32}$ film the phase transition varies from the metastable δ-Cr(N,C) to orthorhombic chromium carbonitride $Cr_3(C_xN_{1-x})_2$ phase up to 800ºC and then to chromium carbide phase. No chromium nitride phases were detected in spite of the similar N and C contents after the deposition. The Cr-C coating recrystallizes into a mixture of carbide phases, mainly Cr_3C_2 and $Cr_{23}C_6$ after 1000ºC annealing treatment.

***Keywords*:** Arc Evaporation, Chromium Nitride, Carbonitride Coatings, Thermal Stability, HTXRD.

1. INTRODUCTION

ACCEPTED MANUSCRIPT

Chromium nitride coatings, which exhibit high hardness and excellent wear, corrosion and oxidation resistance, have been extensively used as protective coating on various tools and dies [1,2]. The oxidation resistance could be considered as the dominant factor for the successful application at elevated temperature conditions. The high oxidation limit of CrN coatings, typically about 700°C [3], was attributed to the formation a protective Cr_2O_3 layer.

Ternary Cr-X-N coatings were prepared with the goal to improve the oxidation resistance and the tribological properties at elevated temperature. Compared to other alloying elements, such as Al [4,5], Ti [6], Si [7], V [5] or B [8], Cr-C-N has been relatively less studied. Cekada *et al.* [9] analyzed Cr-C-N coatings deposited by evaporation. The films were subjected to oxidation tests showing the formation of a thin chromium oxide layer on the top followed by a nitrogen-rich layer demonstrating that nitrogen diffused towards the surface [9]. The microstructure and the thermal stability of arc-deposited Cr-C-N system were complexly analyzed by Almer *et al.* [10]. The comparison of the tribological properties between CrN and Cr-C-N coatings [11] showed the advantage of the later; however, the difference in the friction coefficient and the wear rate is only minimal. In our previous study [12], Cr-C-N coatings were tribologically tested *in situ* up to 500 ºC showing that the wear rate was almost independent on the temperature and lower than that of CrN coatings deposited and tested under similar conditions. Thus, in the present paper the thermally induced phase transitions of Cr-N, Cr-C-N and Cr-C coatings have been undertaken to infer the necessary knowledge to support the conclusion drawn in our previous studies [12, 13].

2. EXPERIMENTAL PROCEDURES

ACCEPTED MANUSCRIPT

Three series of Cr-based coatings were deposited onto high-temperature resistant Fecralloy substrates (72.8% Fe, 22% Cr, 5% Al, 0.1% Y, 0.1% Zr - Goodfellow) by cathodic arc evaporation from two rectangular cathodes using the aforementioned apparatus system [13]. The arc parameters were kept constant for all depositions: the current 80A, the substrate bias -70V and the substrate temperature 350°C. The chromium was evaporated from a Cr target (99.8% purity) in N_2 (99.999% purity) and C_2H_2 (99.6% purity) atmospheres. For binary Cr-N and Cr-C coatings a partial pressure reactive gas of 0.17Pa was set up at a constant value of 100sccm, while for Cr-N-C films the flow of acetylene was fixed at 48sccm. The corresponding increase of the total pressure from 0.17 to 0.20 Pa was measured by a capacitance manometer Leybold CERAVAC Transmitters CTR/91.

High temperature X-ray diffraction (HTXRD) measurements were done using a Philips X' Pert diffractometer with cobalt radiation (K_α = 0.178897nm) in Bragg-Brentano geometry. The samples (12x10mm) were fixed on a Pt plate and heated from RT up to 1000ºC in steps of 100ºC. The heating rate was 40ºC/min between each temperature step followed by maintenance of ~20min for XRD acquisition in 35-60º range. The samples were cooled down to RT and new XRD patterns were acquired in the range 20-110º. The analyses were performed in a vacuum chamber HT16, coupled to the diffractometer and specially designed for *in-situ* analysis. The experiments were performed under continuous gas (Ar-5%H_2) flux at low pressure (1-10 Pa) after evacuating the chamber down to a value lower than 10^{-3} Pa. The measured profile scans were deconvoluted by Origin program, assuming to be Voigt functions to yield the peak position, integrated intensity and integrated width (IntW). These parameters allow calculating the interplanar distance ($\boldsymbol{d_{hkl}}$), preferential orientation and grain size **(ϕ),** using the Scherrer formula, respectively.

ACCEPTED MANUSCRIPT

A Cameca SX-50 Electron Probe Microanalysis (EPMA) apparatus was used to determine the chemical composition of the coatings.

3. Results and Discussion

Fig. 1 to 3 present the *in-situ* XRD structural evolution up to 1000 ºC of the three Cr-based coatings. The XRD patterns before and post annealing, acquired at RT in [20-110º] 2θ range, are also shown. The compositions investigated are summarized in Table 1. To facilitate reading, the coatings were denominated according to their chemical composition measured by EPMA, e.g. $Cr_{60}N_{40}$ is coating with 60 and 40 at.% of chromium and nitrogen, respectively.

The structure of the post-deposited binary Cr-N coating is dominated by the hexagonal β-Cr_2N [ICDD 35-0803] with a mean crystallite size of 12nm and a preferred (300) orientation. Besides nitride phase, also bcc α-Cr phase is detected in all coatings. This phase can be attributed to small Cr-rich droplets. This phenomenon is a characteristic of Cr-based coatings deposited by arc-evaporation [10]. XRD analysis, fig. 1a), reveals that the β-Cr_2N phase is thermally stable up to 1000 ºC. The only remarks are: (i) the narrowing of the peaks and (ii) the shift towards the equilibrium position with increasing temperature in comparison to the post-deposition state. These two effects could be understood more clearly by analyzing simultaneously fig.1b) and fig. 4. This last one shows the *in situ* structural parameters, calculated after peak fitting of corresponding (110) and (111) planes. The interplanar distance is increasing as a function of the annealing temperature up to 700ºC followed by an opposite trend for higher temperatures values. The first trend is well understood due to the lattice expansion under the heating effect (α_{CrN}=2.3x10^{-6} ºC [14]). In this temperature range only small structural rearrangements of a typical recovery process could exist. This

ACCEPTED MANUSCRIPT

process becomes increasingly more intense at 700ºC as shown by the decrease in the interplanar distance (second trend of structural parameters variation in Fig. 4), suggesting stress relaxation and loosing of either the interstitial contaminant elements or the exceeding N from the Cr-N structure [15]. No significant crystallite size variation is observed during heating from RT to 800 ºC. For higher temperatures, the β-Cr_2N peaks become narrower, more intense and the preferential orientation changes from (300) to (110), features characteristic of a recrystallization and grain growth processes. However, even though the grain grows, the $Cr_{60}N_{40}$ film does not loose its nano-characteristics, presenting a mean grain size of 34nm after *in-situ* tempering. These results are better than those reported for CrN coatings, which decompose into β-Cr_2N by N_2 release at temperatures as low as 400ºC [16-18].

The addition of carbon to binary Cr-N films changes the as-deposited structure (compare fig.1a) with fig.2a)). The replacement of N by bigger C atoms increases the local stresses and leads to the instability of the hexagonal nitride phase in addition to a strong decrease of the film crystallinity. The $Cr_{41}N_{27}C_{32}$ film presents, after deposition, a broad and low intensity XRD patterns with a mean feature size of only 4nm, characteristic of a quasi-crystalline or nanocrystalline structure. Taking into account the 2θ maximum peak position, the *d* values obtained after peak fitting match quite well with the fcc-CrN [ICDD 76-2494] structure. Thus, the as-deposited structure of Cr-N-C is dominated by a metastable cubic phase similar to that reported in others works [9,10] and denominated as δ–Cr(C,N) phase. After annealing at 1000ºC, the coating is completely crystallized presenting mainly a mixture of Cr_3C_2 [ICDD 71-2287] and $Cr_3(C_{0.92}N_{0.08})_2$ [ICDD 19-0326] phases, both from the orthorhombic system (fig. 2a)). No nitride phases were detected in spite of the N and C similar contents after the deposition.

ACCEPTED MANUSCRIPT

During the thermal treatment at increasing temperatures, the initial δ-Cr(C,N) phase remains unchanged up to 600ºC (fig. 2b)). The only remark is the shift of the broad peak position to lower diffraction angles, similar to that observed for Cr-N coating, due to the expansion of the lattice under the heating effect. At 700ºC, well defined XRD peaks can be detected being the new phase indexed as an orthorhombic chromium carbonitride $Cr_3(C_xN_{1-x})_2$: the $Cr_3(C_{0.92}N_{0.08})_2$. The content of this phase increases with further annealing. However, at 900ºC, an interesting occurrence can be detected: the intensity of some $Cr_3(C_xN_{1-x})_2$ peaks increases while others strongly decreases. This behaviour is illustrated in fig.2b (see inset graphic), suggesting a progressive transformation of the carbonitride phase. As the peaks remain in the same position, a phase of the same type should be forming: the orthorhombic Cr_3C_2. This proposal, which needs further investigation, is supported by the N loss detected by EPMA analysis on the remaining non-oxidized part of the coating. Fig.5 illustrates that in an oxide spalled zone (see discussion below) only a small amount of the as-deposited N content was found after 1000ºC. It is reported that $Cr_3(C_xN_{1-x})_2$ are metastable crystallographic structures being stable only at high temperatures and/or under high N_2 pressure [19]. Thus, the N content loss could be the driving force for the Cr_3C_2 phase formation.

Similarly to Cr-N-C coatings, also in Cr-C system broad and low intensity XRD peaks, with a mean feature size of ~ 4nm, can be detected together with the α-Cr phase (see fig. 3a)). These low order structured films have already been deposited by other authors by arc-evaporation, sputtering or electrodeposition processes [20-24]. The quasi-crystalline phase is stable up to 600ºC, starting to recrystallize at 700 ºC in the Cr_3C_2 orthorhombic form (see the structural evolution in fig.3b)). Further annealing leads to the formation and growth of another chromium carbide, the fcc-$Cr_{23}C_6$ [ICDD-85-1281]. This phase transition can be expected since originally the C content is not

ACCEPTED MANUSCRIPT

enough to satisfying the stoichiometry of Cr_3C_2 (33at.% against 40at.%). Thus, the tendency for equilibrium requires the formation of a new carbide phase with lower C-content, as is the case of $Cr_{23}C_6$. The occurrence of $Cr_{23}C_6$ instead of Cr_7C_3 (the predicted in the binary Cr-C phase diagram) is probably due to its lower free formation energy. It should be remarked that EPMA analysis carried out in a clear zone after annealing (analogous to that shown in fig. 5) revealed almost exactly the same C content in the coating as post deposition (34.5at.% against the as-deposited 33.3at%).

Finally, it is important to state that no significant structural changes were detected on the cubic α-Cr droplets. As can be seen in fig.6, the crystallite size evaluated from the (110) peak reveals no significant change with increasing temperature up to 1000ºC, whereas the lattice parameter steadily increases. This phenomenon is much more evident for α-Cr droplets than for Cr-N phases (see e.g. fig. 4) due to its higher thermal expansion coefficient (α_{Cr} = $6.5x10^{-6}$ ºC [IUPAC-Periodic Table] against $\alpha_{Cr\text{-}N}$ = $2.3x10^{-6}$ ºC [14]).

The oxidation is a common phenomenon observed in all coatings during the in-situ analysis despite the use of a reducing atmosphere. Even with all precautions (good initial vacuum - 10^{-3} Pa, 2-3 Ar/H_2 flushes before starting the experiments) the formation of an external oxide layer, indexed as Cr_2O_3 phase [ICDD 85-0869], could not be avoided for temperatures higher than 800ºC, as it has already been reported by other authors [25]. For the oxidation reaction progression it is necessary to replace N and C by O in their matrix positions. Since arc-evaporated Cr-N-C films present less compact morphologies than those observed for binary Cr-N and Cr-C coatings, the increased number of paths facilitates the N out-diffusion in small N_2 molecules more easily than C through CO_2/CO gases. The oxidation process seems to be more intense in this coating in comparison to the binary ones, as can be concluded from the comparative

ACCEPTED MANUSCRIPT

analysis of the intensities of the oxide peaks in figs. 1 to 3. During cooling down to RT, oxide layer delamination was detected. Parts of the external oxide layer, shown in fig. 5 for $Cr_{41}N_{27}C_{32}$, spalled out readily in powder form during its subsequent handling. For $Cr_{60}N_{40}$ coating only a change from grey to a green color was observed.

4. CONCLUSIONS

Arc-deposition technique was successfully used to deposit Cr-N, Cr-N-C and Cr-C coatings. The following conclusions can be drawn from the HTXRD analysis of these films:

i) Hexagonal β-Cr_2N is the major phase deposited for 40at.%N coatings, being stable up to 900ºC before recrystallization and grain growth takes place. The mean grain size is only 34nm after treatment.

ii) The deposition with N_2 and C_2H_2 reactive gases leads to quasi-crystalline Cr-based coatings with feature size of only 4nm. The as-deposited metastable δ-Cr(C,N) phase remains unchanged up to 600ºC. Further annealing induces phase transition from chromium carbon nitride $Cr_3(C_{0.92}N_{0.08})_2$ to chromium carbide Cr_3C_2 phase.

iii) For Cr-C coatings the phase transition starts at 700ºC by forming Cr_3C_2; after *in situ* treatment a mixture of carbides phases is presented in accordance to thermodynamic equilibrium.

iv) All coatings exhibit small amounts of Cr-rich droplets, keeping almost constant their structural characteristics during tempering.

v) Finally, the oxidation of the coatings is detected during *in-situ* XRD analysis at temperatures higher than 800ºC, despite the use of reducing atmosphere.

Acknowledgements

ACCEPTED MANUSCRIPT

This work was supported by the Grant Agency of the Academy of Sciences of the Czech Republic through the project KJB201240701 and by the Ministry of Education of the Czech Republic (project MSM 6840770038).

REFERENCES

[1] P.A. Dearnley, *Wear*, 225–229 (1999) 1109

[2] H. Dong, Y. Sun, T. Bell, *Surf. Coat. Technol*. 90 (1997) 91

[3] H. Mayrhofer, H. Willmann, C. Mitterer, *Surf. Coat. Technol*. 146–147 (2001) 222

[4] J. Vetter, E. Lugscheider, S.S. Guerreiro, *Surf. Coat. Technol*. 98 (1998) 1233

[5] M. Uchida *et al*., *Surf. Coat. Technol.* 177-178 (2004) 627

[6] P. Panjan *et al*., *Surf. Coat. Technol*.98 (1998) 1497

[7] H.Y. Lee *et al*., *Surf. Coat. Technol.* 200 (2005) 1026

[8] B. Rother, H. Kappl, *Surf. Coat. Technol*. 96 (1997) 163.

[9] M. Cekada, P. Panjan, M. Macek, P. Smıd, *Surf. Coat. Technol*. 151-152 (2002) 31

[10] J. Almer, M. Odén, G. Hakansson, *Philosophical Magazine* 84 (2004) 611

[11] E.Y. Choi *et al*., *J. Mater. Process. Tech*. 187-188 (2007) 566

[12] T. Polcar, L. Cvrcek, P. Siroky, R. Novak, *Vacuum* 80 (2005) 113–116

[13] T. Polcar, N.M.G. Parreira, R. Novak, *Surf. Coat. Technol*. 201 (2007) 5228

[14] H. Holleck, *J. Vac. Sci. Technol*. A. 4 (1986) 2661

[15] J. Almer, M. Odén, G. Hakansson, *J. Vac. Sci. Tecnol. A* 18 (1) (2000) 121

[16] C. Heau, R.Y. Fillit, F. Vaux, F. Pascaretti, *Surf. Coat. Technol*. 120 (1999) 200

[17] M. Odén, J. Almer, G. Hakansson, *Surf. Coat. Technol*. 120 (1999) 272

[18] A. Andrievski *et al*., *Thin Solid Films* 261 (1995) 83

[19] E. Bauer-Grosse, *Thin Solid Films* 447-448 (2004) 311

[20] Da-Yung Wang *et al*., *Surf. Coat. Technol.* 120-121 (1999) 622

ACCEPTED MANUSCRIPT

[21] J. Esteve, J. Romero, M. Gómez, A. Lousa, *Surf. Coat. Technol.* 188 (2004) 506

[22] S.C. Kwon *et al*., *Surf. Coat. Technol.* 183 (2004) 151

[23] D.B. Lee, S.C. Kwon, *Mater. Sci. Forum* 510-511 (2006) 418

[24] A. Paul, J. Lim, K. Choi, C. Lee, *Mater. Sci. Eng*. A 332 (2002) 123

[25] M.–A. Djouadi *et al*., *Surf. Sci. Technol.* 151 (2002) 510

ACCEPTED MANUSCRIPT

ACCEPTED MANUSCRIPT

TABLE CAPTION

Table 1 - Chemical composition of the Cr-based coatings (at.%).

FIGURE CAPTION

Figure 1 - XRD patterns of $Cr_{60}N_{40}$ sample: a) as-deposited and post annealing structure, b) structural evolution with annealing temperature; o = Cr_2O_3, Pt = platinum plate.

Figure 2 - XRD patterns of Cr-N-C coating: a) as-deposited and post annealing structure, b) structural evolution with annealing temperature; ◊ = δ-Cr(C,N), ● = $Cr_3(C_{0.92}N_{0.08})_2$, * = Cr_3C_2, o = Cr_2O_3, Pt = platinum plate.

Figure 3 - XRD patterns of $Cr_{67}C_{33}$ coating: a) as-deposited and post annealing structure, b) structural evolution with annealing temperature; * = Cr_3C_2, ◘ = $Cr_{23}C_6$, o = Cr_2O_3, Pt = platinum plate.

Figure 4 - Evolution of the structural parameters of the β-Cr_2N phase as a function of *in-situ* XRD annealing temperature.

Figure 5 - SEM surface top morphology of $Cr_{41}N_{27}C_{32}$ sample and the respective elemental EPMA maps for chromium and oxygen after thermal treatment; layer 1 = external Cr_3O_2 layer; layer 2 = inner non-oxidised coating.

Figure 6 - Evolution of the structural parameters of the bcc α-Cr phase as a function of *in-situ* XRD annealing temperature.

ACCEPTED MANUSCRIPT

Table 1

Sample	Cr	N	C	O
$Cr_{60}N_{40}$	60.1	39.7	0.0	0.2
$Cr_{41}N_{27}C_{32}$	41.6	26.8	31.6	0.0
$Cr_{67}C_{33}$	66.5	-	33.3	0.2

ACCEPTED MANUSCRIPT

ACCEPTED MANUSCRIPT

Figure 1

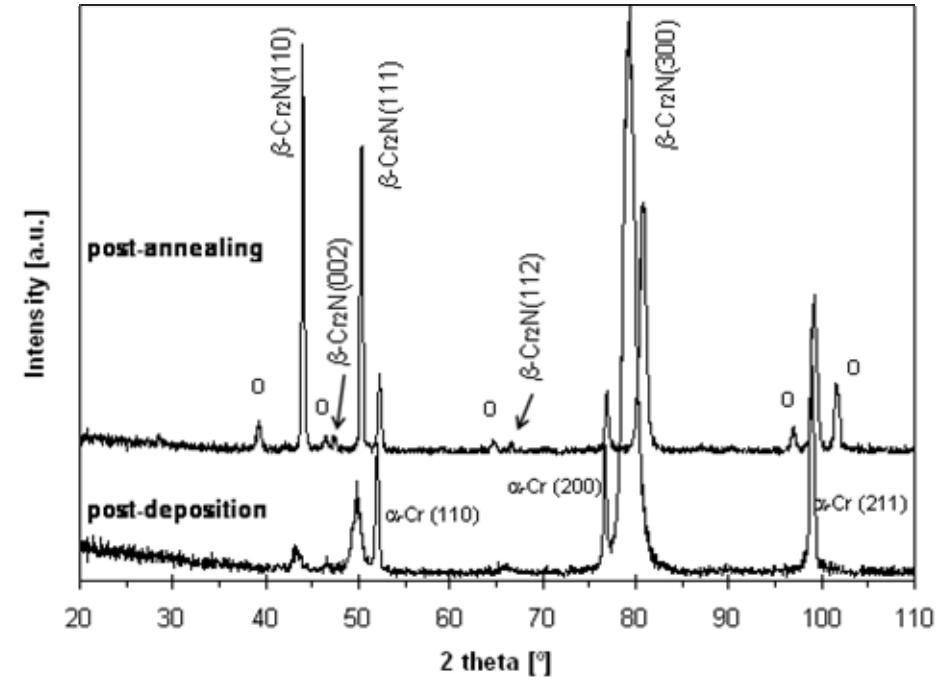

a)

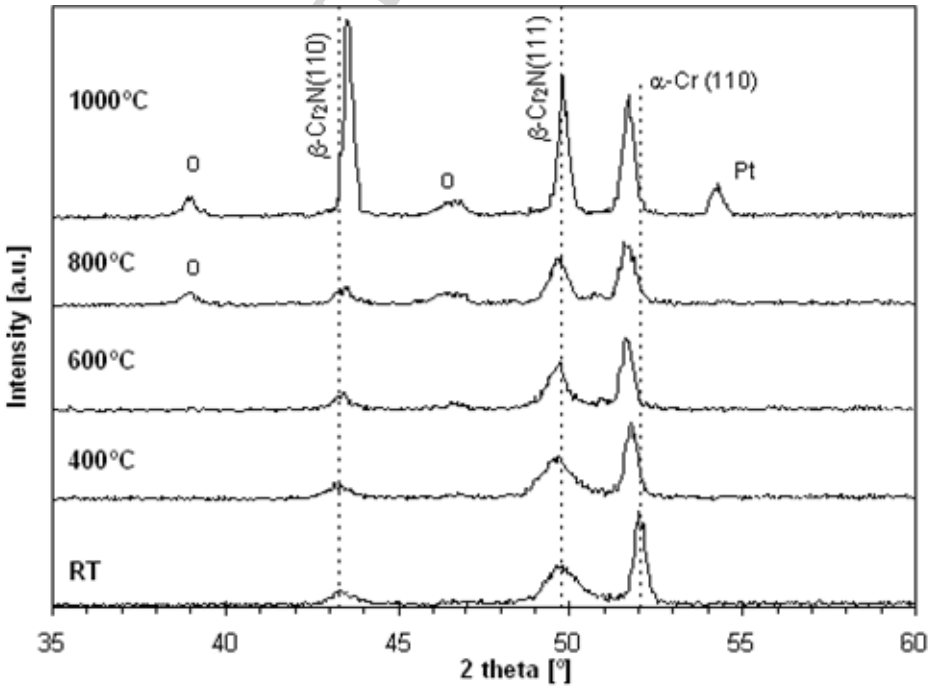

b)

ACCEPTED MANUSCRIPT

Figure 2

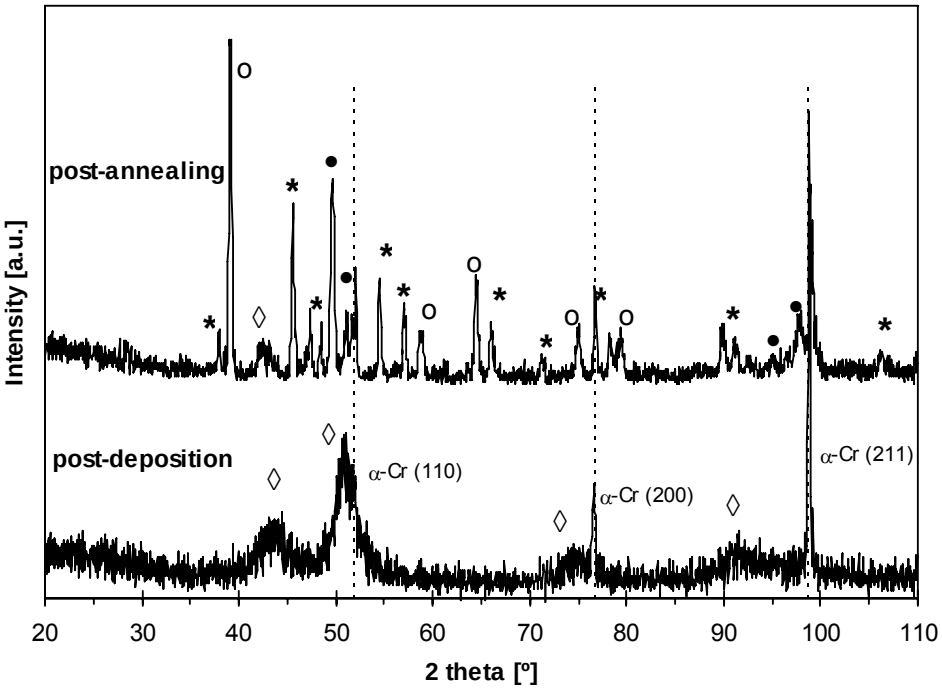

a)

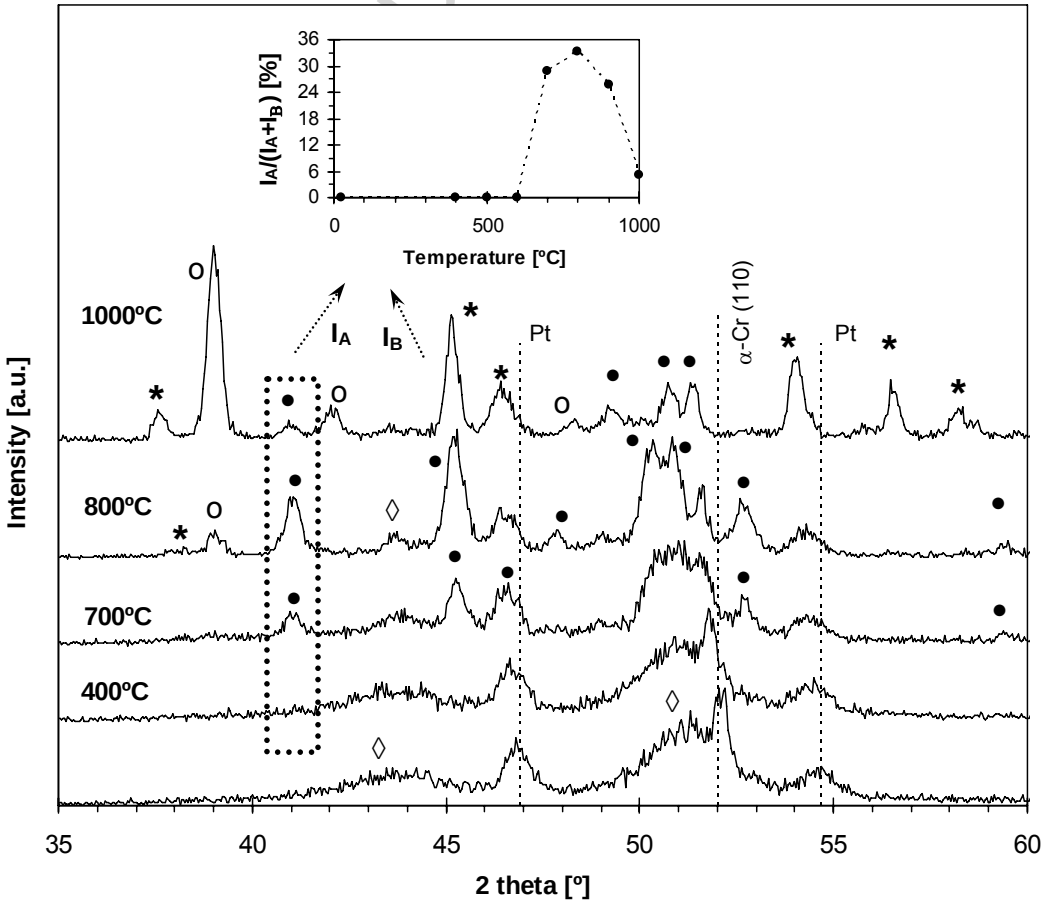

b)

ACCEPTED MANUSCRIPT

Figure 3

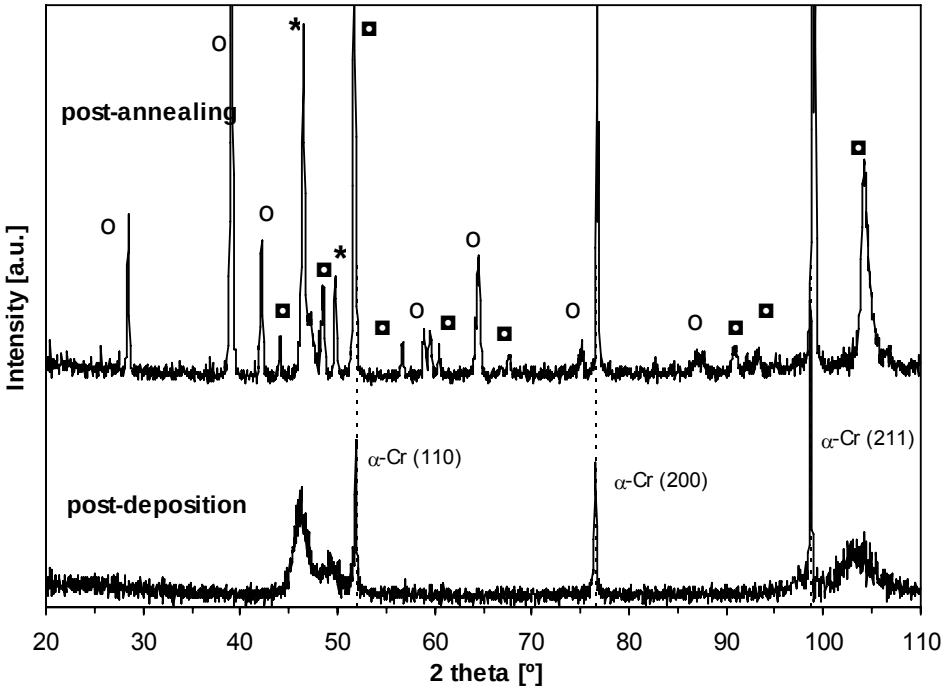

a)

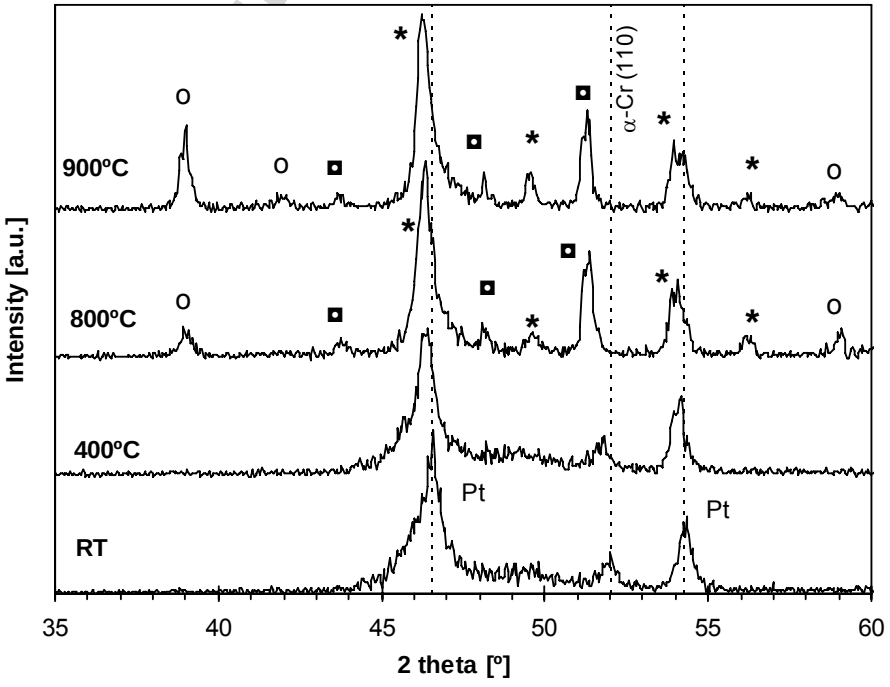

b)

ACCEPTED MANUSCRIPT

Figure 4

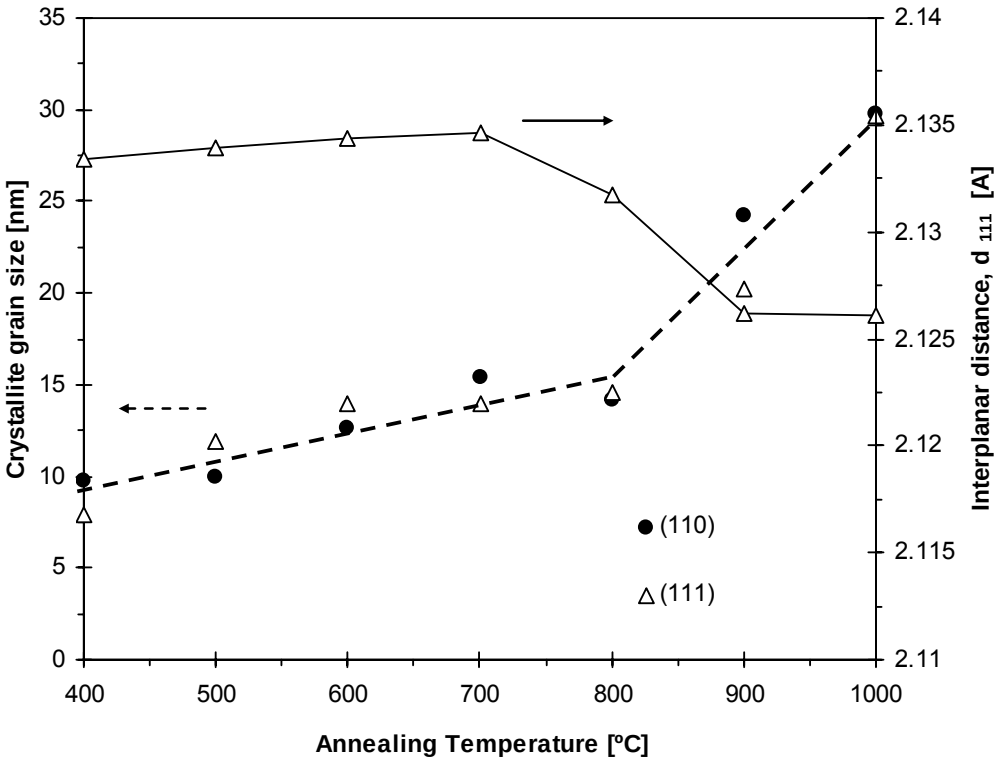

Figure 5

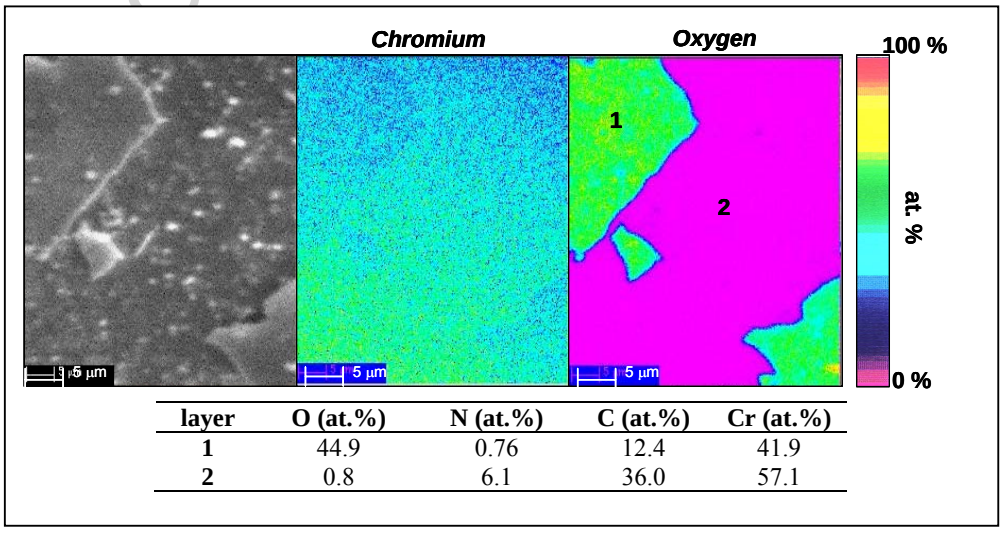

layer	O (at.%)	N (at.%)	C (at.%)	Cr (at.%)
1	44.9	0.76	12.4	41.9
2	0.8	6.1	36.0	57.1

ACCEPTED MANUSCRIPT

Figure 6

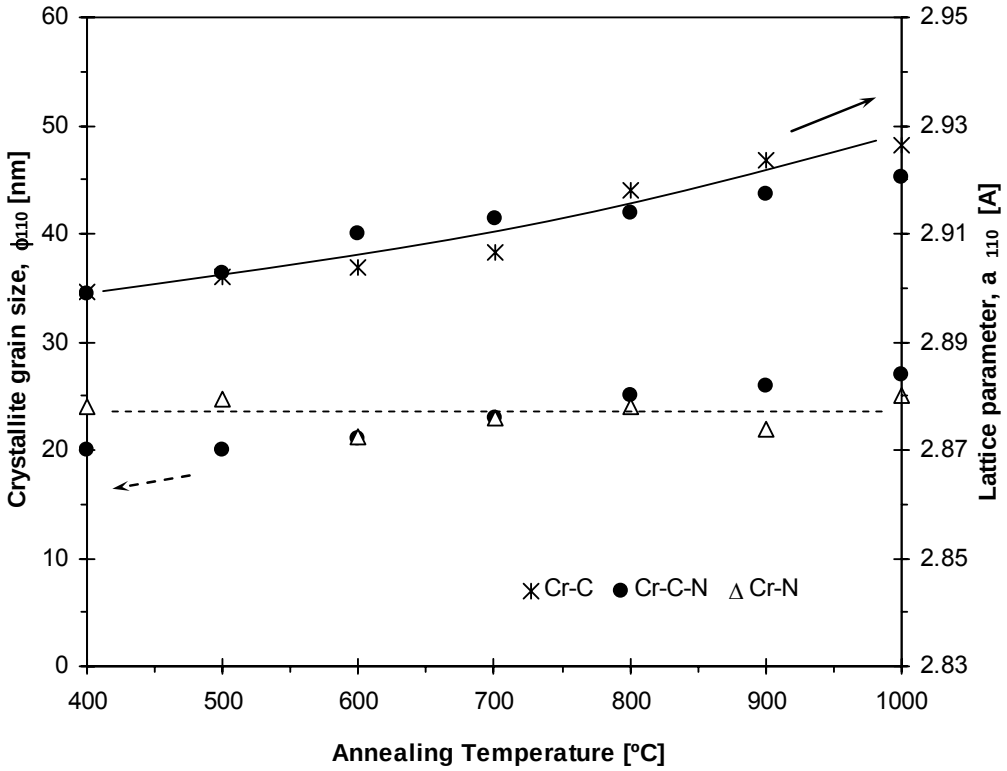

ACCEP